Icarus 283 (2017) 343–351

Contents lists available at ScienceDirect

Icarus

journal homepage: www.elsevier.com/locate/icarus

Space weathering effects in Diviner Lunar Radiometer multispectral infrared measurements of the lunar Christiansen Feature: Characteristics and mitigation

Paul G. Lucey[a,*], Benjamin T. Greenhagen[b], Eugenie Song[c], Jessica A. Arnold[d], Myriam Lemelin[a,e], Kerri Donaldson Hanna[d], Neil E. Bowles[d], Timothy D. Glotch[f], David A. Paige[g]

[a] Hawaii Institute of Geophysics and Planetology, University of Hawaii at Manoa, 1680 East West Road, Honolulu, 96822 HI, USA
[b] Johns Hopkins University Applied Physics Laboratory, 11101 Johns Hopkins Rd. Laurel, 20723 MD, USA
[c] Jet Propulsion Laboratory, 4800 Oak Grove Drive Pasadena Mail Stop 264-623, CA 91109, USA
[d] Atmospheric, Oceanic and Planetary Physics, University of Oxford, Parks Road, Oxford OX1 3PU, United Kingdom
[e] Department of Geology and Geophysics, University of Hawaii at Manoa, 1680 East West Road, Honolulu, 96822 HI, USA
[f] Department of Geosciences, Stony Brook University, Stony Brook, NY 11794-2100, USA
[g] Deptartment of Earth, Planetary and Space Science, University of California Los Angeles, Los Angeles, 90095 CA, USA

ARTICLE INFO

Article history:
Received 30 June 2015
Revised 27 April 2016
Accepted 5 May 2016
Available online 11 May 2016

Keywords:
Moon
Solar wind
Infrared observations
Moon, surface

ABSTRACT

Multispectral infrared measurements by the Diviner Lunar Radiometer Experiment on the Lunar Renaissance Orbiter enable the characterization of the position of the Christiansen Feature, a thermal infrared spectral feature that laboratory work has shown is proportional to the bulk silica content of lunar surface materials. Diviner measurements show that the position of this feature is also influenced by the changes in optical and physical properties of the lunar surface with exposure to space, the process known as space weathering. Large rayed craters and lunar swirls show corresponding Christiansen Feature anomalies. The space weathering effect is likely due to differences in thermal gradients in the optical surface imposed by the space weathering control of albedo. However, inspected at high resolution, locations with extreme compositions and Christiansen Feature wavelength positions – silica-rich and olivine-rich areas – do not have extreme albedos, and fall off the albedo- Christiansen Feature wavelength position trend occupied by most of the Moon. These areas demonstrate that the Christiansen Feature wavelength position contains compositional information and is not solely dictated by albedo. An optical maturity parameter derived from near-IR measurements is used to partly correct Diviner data for space weathering influences.

1. Introduction

Thermal infrared spectroscopy is a powerful tool for characterizing the surfaces of objects in the inner solar system; the major rock-forming silicates and other minerals that make up their surfaces exhibit unique vibrational spectral signatures in the region of thermal emission from about 5 to 50 μm. Among the spectral features present in this wavelength region is a peak in thermal emission called the Christiansen Feature (CF) that occurs at wavelengths somewhat shorter than the fundamental infrared vibrational features associated with each mineral, near a wavelength where the real index of refraction of the mineral passes through unity. At this wavelength the spectral emissivity of the surface is at a maximum, and as its position is correlated with the position of the associated fundamental vibration, the emission maximum contains diagnostic information regarding the minerals present. The position of the feature is correlated with the average silica content of minerals, with high-silica minerals exhibiting the shortest Christiansen Feature peak positions, and of the common silicates, olivine shows the longest peak position (Logan et al., 1973). Therefore, thermal infrared spectroscopy using the CF is sensitive both to highly transparent iron-poor silica-rich minerals and glasses not directly perceptible to near-IR spectroscopy, materials that are diagnostic of evolved rock types identified in the lunar returned sample collection, and provides an independent estimate of the more common lunar silicates.

* Corresponding author. Tel.: +1 8082212135.
E-mail address: lucey@higp.hawaii.edu (P.G. Lucey).

http://dx.doi.org/10.1016/j.icarus.2016.05.010

The Diviner Lunar Radiometer Experiment (Diviner) features three spectral bands designed to characterize the position of the Christiansen Feature. Diviner is a 9 band multispectral infrared radiometer on NASA's Lunar Reconnaissance Orbiter that has mapped most of the lunar surface at wavelengths from 0.3 to 400 μm at about 200-meter resolution. Among these bands are three narrow channels that span the wavelength ranges 7.55–8.05, 8.10–8.40, and 8.38–8.68 μm (Diviner channels 3, 4, and 5) that are used to estimate the position of the Christiansen Feature using a 3-point parabolic fit to the emission at the three bands (Greenhagen et al., 2010).

In the decades before the launch of the Lunar Reconnaissance Orbiter, it was suggested that thermal IR spectroscopy would be a uniquely powerful tool for lunar remote sensing in part because evidence indicated this technique was less susceptible to the known optical effects of exposure of the lunar surface to space (Nash et al., 1993). At the visible and near-IR wavelengths that are widely used for lunar mineralogic remote sensing, spectra of lunar materials are strongly influenced by exposure to the space environment, a process known as space weathering (Pieters et al., 2000; Hapke 2001). Compared to spectra of the pulverized lunar rock that might be expected on the impact-dominated lunar surface, lunar regolith is darker and its spectra exhibit weakened spectral absorption features and a strong decrease in reflectance toward shorter wavelengths (Fischer and Pieters, 1994). These effects are now attributed to a combination of the optical properties of extremely fine-grained iron particles – nanophase iron – in vapor deposits on lunar grain surfaces produced by solar wind sputtering and micrometeoroid impact, and by ubiquitous dark glass produced by micrometeoroid impact that can comprise up to 30 wt. % of surface soils. However, two studies had suggested that space weathering would have less impact on thermal emission spectra than that found in spectroscopy at shorter wavelengths. Nash and Salisbury (1991) showed that the position of the Christiansen Feature of lunar analog minerals was not affected when the materials were vitrified, so the conversion of minerals to impact glass was not expected to cause a spectral effect. In an infrared spectral study of lunar soils returned by the Apollo Program, Salisbury et al. (1997) showed that the position of the Christiansen Feature in soils was not correlated with a widely accepted measure of space exposure. Together, these studies led to the expectation that Diviner measurements of the position of the Christiansen Feature would be little affected by space weathering, and so provide a straightforward indicator of the mineral composition of the lunar surface.

Once global data became available from Diviner, it became evident that the Christiansen Feature on the lunar surface was affected by space weathering [Lucey et al., 2010; Greenhagen et al., 2010; Glotch et al., 2015]. Young features such as interiors, ejecta and ray deposits of the craters Tycho and Jackson show Christiansen Feature positions at systematically shorter wavelengths than their more space weathered surroundings, as do deposits of the innumerable other young rayed craters. Lunar swirls, commonly thought to form as a result of inhibition of the space weathering process, also show shorter Christiansen Feature positions than the terrains upon which they are imprinted.

Away from fresh features, the underlying composition was also revealed by the position of the Christiansen Feature. As expected, the lunar highlands as a whole exhibit Christiansen Feature positions at short wavelengths characteristic of their very high feldspar contents, while the lunar maria show Christiansen Feature positions at longer wavelengths indicative of their more mafic lithologies.

The dependence of the Christiansen Feature on degree of space weathering is a partial impediment to its use for compositional estimation, in particular in regions where the degree of space exposure is highly variable, such as in the vicinity of young craters or on steep slopes where mass wasting may reveal relatively unweathered material. This paper quantifies the degree to which space weathering affects the Christiansen Feature, and presents mitigation techniques that allow the effects of space weathering to be normalized in order to examine the underlying composition as revealed by the Christiansen Feature. Finally, we will present and discuss hypotheses for the unanticipated space weathering dependence revealed by the Lunar Reconnaissance Orbiter mission's Diviner experiment.

2. Data sources

Diviner's three channels near 8 μm are used to estimate the wavelength of the Christiansen Feature. We used PDS-archived calibrated radiances from these three 8 μm-region channels to calculate effective emissivity and then fit the three emissivity values with a parabola. The wavelength maximum of the parabola is the estimated Christiansen Feature wavelength (Greenhagen et al., 2010). Although Diviner-derived Christiansen Feature values deviate systematically from the Christiansen Feature emissivity maximum wavelength determined from high-resolution spectra, these deviations are well-understood (Greenhagen et al., 2010, SOM). Of greater concern are variations in Christiansen Feature values caused by illumination and topography. Our data were "photometrically" corrected by projecting the data onto a high-resolution topographic grid, calculating photometric geometry, and applying the most up-to-date empirical correction methodology (Greenhagen et al., 2010; 2011). Diviner data were binned at 32 pixel per degree to produce global maps of Christiansen Feature values for latitudes below 60 degrees, using all data collected from LRO's nominal 50 km mapping orbit (September 15, 2009 through December 11, 2011).

The degree of space weathering is quantified using the OMAT parameter of Lucey et al., 2000 applied to the multispectral data from the Clementine mission at 32 pixel per degree (Nozette et al., 1994).

We also compare the position of the Christiansen Feature to visible albedo measurements by the Japanese space agency (JAXA) lunar remote sensing satellite known as Kaguya or SELENE. Among its instruments, that satellite carried a multispectral camera that included a band at 750 nm and mapped the lunar surface at a spatial resolution of about 20 m (Ohtake et al., 2008). Here we use a mosaic of those data, photometrically corrected, and downsampled to 32 pixels per degree to compare to the Diviner measurements.

For some figures we use the Christiansen Feature wavelength positions reported by Salisbury et al., 1997 for lunar soils, and composition and space weathering analyses for the same soils by Morris, 1978.

Additional thermal infrared emissivity measurements of two Apollo 16 lunar soils of similar composition, 66031 and 67701, but with differing degrees of exposure to space weathering were measured under ambient and simulated lunar conditions are used. These laboratory measurements were made in the Asteroid and Lunar Environment Chamber at Brown University and are further characterized by Donaldson Hanna et al. (this volume). For ambient or Earth-like measurements, samples are heated from below to 405 K in an environment chamber at ambient temperature and filled with ~1000 mbars of dry nitrogen. Lunar conditions are simulated by heating the samples from below to 405 K and from above with a solar-like halogen lamp in a cooled environment chamber (~85 K) in vacuum.

3. Results

Fig. 1 shows the Christiansen Feature wavelength position in grayscale plotted from 8 to 8.5 μm, covering all longitudes and latitudes from 60° S to 60° N. Large young rayed craters exhibit

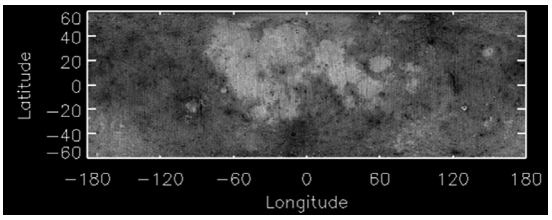

Fig. 1. Grayscale image of the Christiansen Feature wavelength position in grayscale plotted from 8 to 8.5 μm. Note that in the lunar highlands, dark features are associated with large young Copernican rayed craters including Tycho (43.31°S 11.36°W), Jackson (22.4°N 163.1°W) and Giordano Bruno (35.9°N 102.8°E).

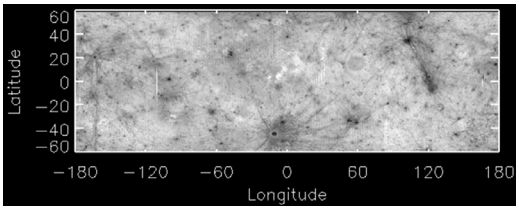

Fig. 2. Global image of the optical maturity parameter OMAT (Lucey et al., 2000) displayed as a negative, from 0.35 (black, immature) to 0.1 (white, mature) units. Maturity anomalies are present at the same locations as found in the global CF image (Fig. 1).

local Christiansen Feature lows; Tycho at (43.31°S 11.36°W), Jackson at (22.4°N 163.1°W) and Giordano Bruno (35.9°N 102.8°E) are particularly prominent, but the dark mottling throughout the highlands is also due to the presence of fresh exposures of small craters. For comparison, Fig. 2 shows the optical maturity (OMAT) parameter of Lucey et al., 2000, plotted as a negative for consistency with the Christiansen Feature image in Fig. 1. The ray patterns for most of the large Copernican craters seen in the Christiansen Feature image are mirrored in this optical maturity parameter.

Gold (1955) argued that a process operated on the Moon to alter its surface. He showed that among the population of large morphologically fresh craters, only the stratigraphically youngest exhibited bright rays, indicating that rays were removed over time. These arguments can be applied equally to the Christiansen Feature data set. Without exception, the same morphologically fresh craters that exhibit bright rays at visible wavelengths show local negative Christiansen Feature anomalies, that is, exhibit values that are shorter in wavelength than that of the surrounding background. The presence of rays in Christiansen Feature data for the large young craters on the Moon is strong evidence for the influence of space weathering on the lunar surface.

Fig. 3 presents a histogram of Christiansen Feature positions for the global data set, with the positions of the stratigraphically youngest (Copernican and Eratosthenian) large craters superimposed. The large rayed craters have Christiansen Feature wavelengths shorter than both the typical global CF value, and the shortest CF exhibited by Eratosthenian craters. (We exclude those craters with rays that persist owing to compositional contrast such as Copernicus, Hawke et al., 2004). The Christiansen Feature wavelength values are the average of a box centered on each crater, two crater diameters in width, to encompass the crater interior and continuous ejecta. The mean difference in CF values between nonmare Eratosthenian craters and nonmare Copernican craters is 0.052 +/− 0.035. The mean CF value of the nonmare Eratosthenian craters (8.148 +/− 0.02) is similar to the mode of the global CF histogram (8.155).

Superimposed on these putative local space weathering anomalies are background variations in the position of the Christiansen Feature that were anticipated prior to Diviner measurements: the feldspar-rich highlands exhibit short Christiansen Feature wavelengths, while the more pyroxene-rich lunar maria show relatively long Christiansen Feature positions (Greenhagen et al., 2010). The approximate mode of the Christiansen Feature position for the lunar maria is about 8.25 μm while the approximate mode for the lunar highlands is about 8.15 μm, a difference of about 0.1 μm. The range of the space weathering influence on the Christiansen Feature position observable at the scale of Fig. 2 (~0.05, see above) half that imposed by the compositional difference between the two major lunar surface compositional units. (Note that for pure minerals the compositional differences are much larger than the space weathering effect. For example, anorthite has a Christiansen Feature emissivity maximum wavelength at about 7.85 μm, augite is at 8.15 μm and forsterite is at about 8.65 μm. Mixtures mute the variations but more pure units will have greater contrast as discussed below.) Nevertheless, the space weathering effect must be taken into account when using Christiansen Feature wavelength positions for compositional estimates.

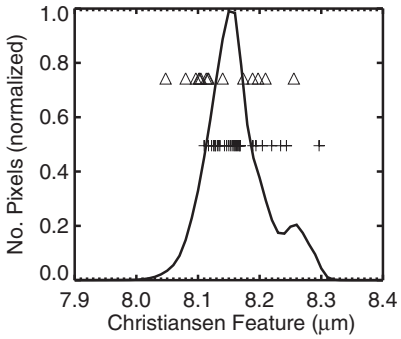

Fig. 3. Histogram of CF values for the global data shown as the solid line. The histogram shows a "long tail" toward short values representing immature locations; the bump at 8.25 μm represents the lunar maria. Triangles and plus signs are the CF values for all Copernican and Eratosthenian craters between 40 and 110 km in diameter respectively (y value is not significant). The Copernican craters extend to short CF values; these examples are the rayed craters. Craters with longer CF values occur in the lunar maria.

4. Discussion

These results raise two questions: what is the origin of the unanticipated space weathering effect, and what can be done to mitigate these effects in compositional applications of Diviner Christiansen Feature data?

4.1. Origin of space weathering effects

We have formulated two hypotheses regarding the origin of the space weathering effects seen in Diviner data: The first is that the Christiansen Feature is influenced both by the underlying composition of the minerals present, and the physical and compositional changes associated with space weathering, analogous to the effects of space weathering on spectral properties at visible and near-IR wavelengths. The second is that the Christiansen Feature position is dictated by albedo-dominated variations in the thermal gradient in the optical surface, consistent with the general inverse correlation of the Christiansen Feature wavelength position and visible albedo. Thermal gradients are known to have a powerful influence on Christiansen Feature wavelength positions (e.g. Logan et al., 1973; Henderson and Jakosky, 1997; Donaldson Hanna et al., this volume) and albedo is reasonably assumed to influence the thermal gradient of the surface, suggesting a connection between Christiansen Feature and albedo.

4.1.1. Composition physical effects

Extreme changes in regolith properties occur with space weathering on the Moon. A lava flow, impact melt deposit or other

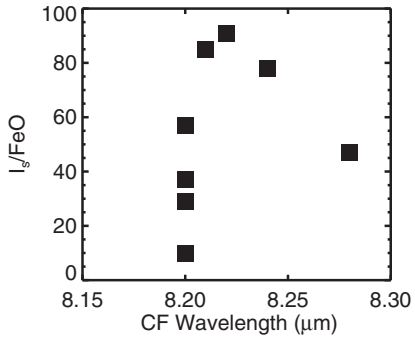

Fig. 4. Relationship between CF position and space weathering exposure for 8 soils from Apollo 16. CF data from Salisbury et al., 1997. I_s/FeO data from Morris, 1978. I_s/FeO is the most widely used indicator of exposure of lunar soil to the space environment, and is the abundance of nanophase iron (expressed in arbitrary units) normalized to the bulk soil iron content. There is no significant correlation between these quantities, despite the large range in soil exposure. For context the full range of I_s/FeO over all lunar soils is 1 to 110 (Morris 1978).

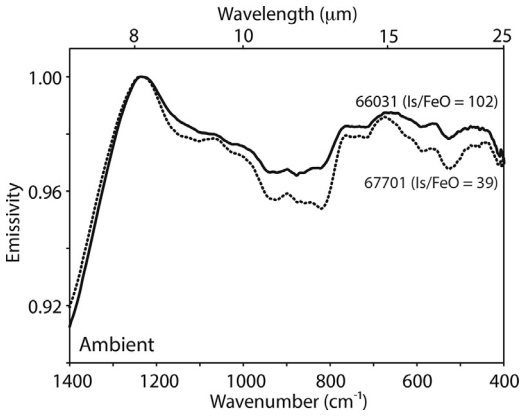

Fig. 5. Thermal infrared emission spectra of lunar soils 66031 (solid) and 67701 (dashed) measured in air (Donaldson-Hanna et al., submitted for publication). Despite major differences in space weathering exposure (I_s/Feo 39 vs. 102), these soils share nearly identical CF positions (peak near 8 μm) though they show important differences in contrast at other wavelengths. This indicates little sensitivity of the Christiansen Feature position to the compositional and physical changes with space weathering exposure.

unaltered rock on the lunar surface will be pulverized by meteorite impact and in its fine particulate state be subject to solar wind sputtering and implantation, as well as micrometeoroid bombardment (e.g. Hapke 2001). Both of these phenomena cause local vaporization of grain surfaces and leave amorphous vapor-deposited coatings on surrounding mineral grains. These coatings are unusual in composition relative to the source material, and contain iron spherules with diameters of tens of nanometers (Keller and McKay, 1997; Pieters et al., 2000). In the visible and near-IR, the nanophase iron spherules have a powerful optical effect causing darkening of the surface, weakening of mineral absorption bands and imparting a continuous decrease in reflectance toward shorter wavelengths (Noble et al., 2001).

In addition to vapor-deposited coatings, micrometeoroid impacts also cause local melting, giving rise to small deposits of impact melt glass and mineral fragments called agglutinates. These agglutinates can comprise up to 60 % of highly exposed soil by volume and the glass itself up to 30% by volume (Taylor et al., 2001). The glass is itself dark, being infused with nanophase iron particles that may be gathered from fragments of previously produced vapor deposits remelted in the subsequent impact of a micrometeoroid. These compositional changes are matched by physical changes in grain size, grain size distribution and regolith porosity as rocks and minerals are broken down and glassy agglutinates accumulate.

Despite these large changes, measurements by Salisbury et al. (1997) indicated that there was no obvious correlation between mid-IR spectral properties and soil maturity. Fig. 4 shows this lack of relationship in the data of Salisbury et al. (1997) where no significant correlation is observed between the space exposure parameter I_s/FeO and CF position. I_s/FeO is the most common metric for estimating degree of space exposure in lunar soils – *soil maturity* in the lunar regolith sample literature – and is a measure of the abundance of nanophase iron in the bulk soil, normalized to the bulk iron content of the soil. The abundance of nanophase iron is quantified by the intensity of ferromagnetic resonance in lunar soils and normalized to the iron content because the ultimate source of the nanophase iron is the lunar rock itself. Additional evidence is provided in a paper in this volume. Donaldson-Hanna et al. present thermal infrared spectra of lunar soils and among them are measurements of Apollo soils 67701 and 66031 collected at the Apollo 16 site (sampling stations 11 and 6, respectively). While these soils share very similar compositions (3.97 and 5.8 wt. % FeO respectively, indicating similar feldspar to pyroxene ratios), the extent of their exposure to space is very different. Soil 67701 has an I_s/FeO value of 39 and 66031 has a value of 102. This is a large fraction of the full range of I_s/FeO across all measured lunar soils, which range from 1 to 110 (Morris 1978). The infrared spectra of these two soils collected under ambient conditions are shown in Fig. 5; there is very little difference overall, and little difference in Christiansen Feature wavelength position, consistent with Salisbury et al. (1997). These spectral measurements suggest that the physical and compositional changes accompanying space weathering do not have a strong effect on spectral properties of lunar regolith measured under ambient laboratory conditions, supporting the conclusions of Salisbury et al., 1997.

4.1.2. Thermal gradients

The Salisbury et al. (1997) data, and those in Fig. 5 from Donaldson Hanna et al. (2012b), were obtained under terrestrial ambient conditions. Measurements at $< 10^{-4}$ mbar pressure with a radiative environment simulating that in space – illuminated from above by a roughly solar light source, and with a low temperature background – causes strong changes in the spectral properties of powdered materials (e.g. Logan and Hunt, 1970; Henderson and Jakosky, 1997; Thomas et al., 2012; Donaldson Hanna et al., 2012a). Donaldson Hanna et al. (2012b) measured 67701 and 66031 under simulated lunar radiative conditions with very different results than those obtained under terrestrial conditions (Fig. 6). Measured under simulated conditions, the more space-weathered soil shows a Christiansen Feature wavelength position at a longer wavelength than the less weathered soil, consistent with the sense of the Diviner observations, though the magnitude of the shift (0.09: 8.02 μm for 66031 and 7.73 μm for 67701) is twice the difference in CF between Copernican nonmare craters and the mature background. This may simply indicate that 66031 is less mature than the regolith of the population of Copernican craters. The spectra of the soils measured under simulated lunar conditions also feature a substantial decrease in emissivity (increased spectral contrast) at longer wavelengths, which could potentially be observed in Diviner channels 6 (12.5–25 μm) and 7 (25–50 μm).

The major physical difference between samples measured at ambient and simulated lunar conditions is the presence of a strong thermal gradient in the optical surface enabled by the very low conductivity of lunar soils in a vacuum. Under terrestrial conditions vigorous gas conduction results in isothermal conditions in the optically active upper layer of a regolith surface; in vacuum conduction is limited by the small area of grain-to-grain contact. Henderson and Jakosky (1997) constructed a combined thermal

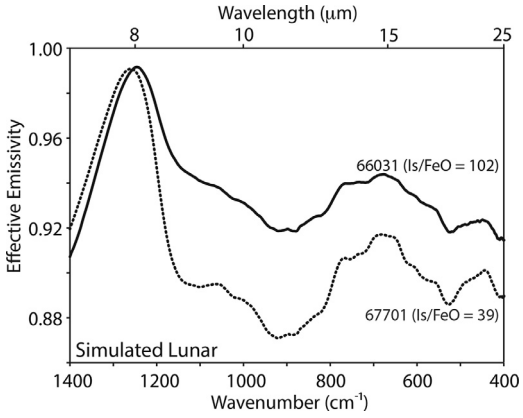

Fig. 6. Spectra of the soils shown in Fig. 5 (66031, solid and 67701, dashed) measured under simulated lunar conditions: under vacuum, with a cold background and heated from above with visible radiation. Strong differences between the two have emerged, including a shift in CF and spectral contrast. The sign of the shift is consistent with Diviner observations of shifts with apparent differences in space weathering.

and radiative transfer model of the thermal and infrared spectral effects of illuminating particulate surfaces from above under varying pressure, and the influence on the thermal emission spectrum of the materials. Using quartz and basalt as test materials, they successfully reproduced the major spectral effects of varying pressure shown in the Logan et al. (1973) experiments; spectral contrast increases greatly with reduced pressure and the Christiansen Feature shifts to shorter wavelengths. In their model these effects arise from the combination of two phenomena. First, because their test materials were more transparent in the visible than in the infrared, energy from the illumination source is deposited more deeply than is accessible to radiative cooling at infrared wavelengths. The consequence is the accumulation of energy below the surface producing a warm layer below a cooler surface layer. This process, called a solid-state greenhouse, was previously recognized and experimentally verified (Dissly et al., 1990). Second, the infrared opacity is strongly wavelength dependent owing to the variation in optical properties of the test materials, causing variations in the depth from which radiation is derived. Where opacity is low, the net emission includes a contribution from the warm layer below the surface and so tends to have higher emission than the isothermal case. As pointed out by Henderson and Jakosky (1997), the result is that the emission spectrum in the presence of a thermal gradient is a product both of the inherent spectral variation in emissivity that gives rise to features in the emission spectrum even in the isothermal case, and also to the degree to which each wavelength samples the thermal profile at depth. Because the infrared opacity generally increases toward longer wavelengths, the net effect is to suppress emission on the long wavelength side of the Christiansen Feature, and increase emission on the short wavelength side, causing a shift of the peak to shorter wavelengths.

The variation in pressure was explored as a variation in thermal conductivity by Henderson and Jakosky (1997). While this aspect of the model explains the experimental results of Logan et al., 1973 and subsequent experiments, the case of varying conductivity with other parameters held constant is not closely analogous to the lunar case, where pressure is constant (zero) but albedo varies.

A comparison of the results of Henderson and Jakosky (1997) for quartz and basalt under the low-pressure (low conductivity) case is relevant. Because the basalt has a much lower albedo than quartz, energy from the illumination source is absorbed over shorter scales than in the former case, and the length scales of absorption and emission are more similar. The consequence was that the model spectral effects of the thermal gradient that are vividly displayed in the quartz case were subdued in the case of the low albedo basalt. Taking the isothermal case as a reference, the CF of the high albedo material (quartz) shifted strongly to shorter wavelengths, while the CF of the low albedo material (basalt) shifted weakly, if at all. This comparison is complicated by the fact that the spectral properties of the basalt are quite different than quartz, and so the lesser shift in wavelength in the basalt cannot be unambiguously attributed to its lower albedo, but the result is of the right sign. The experiments suggest that in the presence of thermal gradients, among surfaces with similar compositions but variable albedo, brighter surfaces ought to exhibit shorter CF positions than darker surfaces, consistent with observations.

If we assume that measurements under ambient conditions reflect the major compositional influences on the infrared spectra, then the Salisbury et al. (1997) and Donaldson Hanna et al. (this volume) results suggest that the physical and compositional changes with space weathering have a minor effect on the inherent optical properties of lunar soils. However, measurements under simulated lunar conditions show space weathering effects that are consistent with the Diviner observations. What is not yet known from laboratory experiments are the relative magnitudes of the thermal gradient and compositional influences. Does albedo entirely dominate the Christiansen Feature position, meaning that Diviner thermal infrared multispectral measurements of the CF simply reflect albedo and are not contributing substantial independent compositional information? We can test this hypothesis using the Diviner data itself.

4.1.3. Albedo-Christiansen feature wavelength correlation

We can falsify the hypothesis that the Christiansen Feature wavelength is solely dictated by the visible albedo by finding major exceptions to the correlation. The most likely exceptions would be found at locations featuring minerals with extreme Christiansen Feature wavelength positions; if albedo controls the Christiansen Feature then these locations should show similar extreme albedos, and fall on the general CF-Albedo trend. Glotch et al. (2010, 2011) reported anomalous spectral shapes associated with extremely short Christiansen Feature positions that they interpreted to be due the presence of silica rich minerals or silica glass. These locations offer a powerful test of the albedo-Christiansen Feature control hypothesis. At the other end of the lunar compositional range, Arnold et al. (submitted for publication) examined lunar areas shown by near-IR reflectance spectral measurements to be rich in olivine, the lunar mineral with the longest wavelength Christiansen Feature position.

We extracted the CF values of these silica-rich and olivine-rich regions from the Diviner data, and albedo from the Kaguya 750 nm albedo mosaic and present them in Fig. 7. Clearly the Si-rich regions fall strongly off the trend, and many of the olivine-rich locations also fall substantially off the trend. Despite the extreme CF values reflective of their unusual compositions, both of these compositional types show relatively unremarkable albedos. This demonstrates that albedo alone does not dictate the position of the Christiansen Feature wavelength.

4.2. Mitigation

The combined effect of composition and space weathering complicates the use of the Christiansen Feature wavelength position for compositional inferences. This situation is not without precedent. Several papers have used visible albedo to estimate iron and aluminum contents of the lunar surface, despite the obvious influence of weathering (e.g. Fischer and Pieters 1995). Similarly, spectral ratios between UV and visible wavelengths have been used to estimate titanium abundances in the lunar maria, also despite

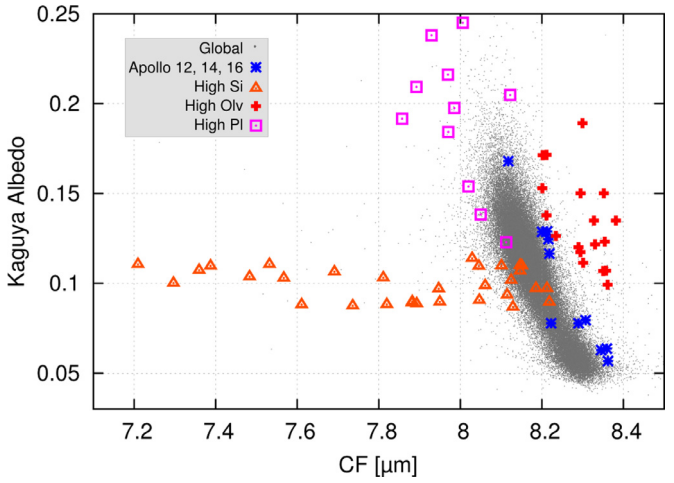

Fig. 7. Dependence of CF position on albedo. Gray dots are global data showing a strong inverse correlation. Orange triangles are high silica regions of Glotch et al., 2010, red crosses are high olivine locations of Arnold et al. (submitted for publication). Purple squares are high plagioclase regions of Donaldson-Hanna et al. 2012a. The high silica regions and high olivine regions demonstrate that albedo does not exclusively determine the CF position. (For interpretation of the references to color in this figure legend, the reader is referred to the web version of this article).

the obvious influence of space weathering on this parameter (e.g. Charette et al., 1974). In both cases users took care to limit analysis to flat surfaces where mass wasting could not act to expose fresh material, and avoid features clearly associated with fresh craters. This approach has been taken with data from Diviner where analysis of the iron content of pyroclastics inferred from Christiansen Feature wavelength positions is limited to level areas with no evidence of significant amounts of fresh unweathered material (Allen et al., 2012). We can estimate the uncertainty in CF position when confining analysis to mature surfaces. Allen et al., 2012 tabulated the CF values for Apollo landing sites. Among the 4 sites where CF values were extracted for mare surfaces with very similar iron contents, the standard deviation is 0.02 μm, much smaller than the 0.1 μm difference between mare and highland.

Lucey et al. (2010) developed an empirical correction to the Diviner data using the optical maturity parameter OMAT (Lucey et al., 2000). The concept was simple. Given a CF that is a combination of space weathering and composition, a properly scaled independent measure of extent of space weathering may be successful at freeing the CF measurement from space weathering influences. The principal metric for success is a visual suppression of the obvious space weathering artifacts at the global scale. Recently Arnold et al. (submitted for publication) used the algorithm of Lucey et al. (2010) to correct CF values for the effect of space weathering. That paper underscored the importance of the ambiguity associated with the Christiansen Feature wavelength position without regard to space weathering. Olivine-rich locations identified by Yamamoto et al. (2010) in near IR spectra data were interpreted by them to be composed of pure olivine in some cases, a strong indicator of the presence of outcrops of the lunar mantle. Arnold et al. showed that without correcting for space weathering, Christiansen Feature wavelength positions also suggested that several of the olivine-bearing locations contained no plagioclase (again, a strong indicator of lunar mantle material). However, application of the space weathering correction of Lucey et al. (2010) resulted in shifting the Christiansen Feature wavelength position of the olivine-bearing locations to shorter wavelengths, leaving no olivine-bearing locations with estimated mineral abundances free of plagioclase, and most containing substantial amounts of plagioclase. Thus a space weathering correction has important implications for the understanding of lunar lithologies.

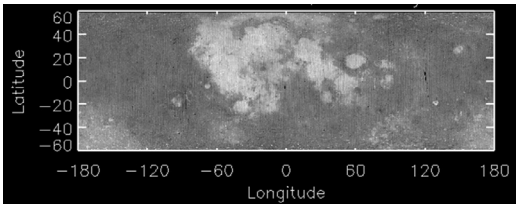

Fig. 8. Global CF image adjusted for space weathering using Eq. 2. The obvious space weathering anomalies associated with fresh craters have been eliminated. Compare with Fig. 1.

Here we revisit the correction of Lucey et al. (2010), update its parameters, and present aspects of its effectiveness. Figs. 1 and 2 show the two parameters of interest–Christiansen Feature position and OMAT. By coincidence, the OMAT scale factor that best removes the obvious effects of large rayed craters from the CF map is 1.0, leading to a base correction is the simple sum of the Christiansen Feature wavelength position and OMAT. Because OMAT is everywhere positive and its addition would shift all the CF values to longer wavelengths, we elected to tie the correction to a known location. At Jackson crater, the lower portion of the central peak is composed of pure anorthosite and for lunar material is relatively fresh (Ohtake et al., 2009). We elected to subtract an offset from the sum of CF+OMAT to make the central peak of Jackson equal to its minimum value (~7.9 μm) that is somewhat similar to the measured value of anorthite under simulated lunar conditions (7.84 μm, Donaldson Hanna et al., 2012a). The penultimate correction is:

$$CF_{Adjusted} = CF + OMAT - 0.285 \quad (1)$$

The CF image adjusted for space weathering is shown in Fig. 8. The strong anomalies at the large young rayed craters have been eliminated successfully.

Note this is somewhat different than the correction used by Arnold et al. (submitted for publication) (offset constant used in that paper was 0.4). This difference does not alter their conclusion that the olivine-rich locations identified by Yamamoto et al. (2010) do not include dunite.

Examined at high resolution, the correction based on OMAT does show some problems that we address below. Fig. 9a shows the CF image for Giordano Bruno, likely the youngest crater of its size on the Moon (Basilevsky and Head, 2012). The interior and continuous ejecta show CF lows, and its distinct ray pattern is also evident. While it is possible this young crater has coincidentally exposed a rich deposit of anorthosite, this is probably unlikely. The OMAT image of the crater is shown in Fig. 9b where similar features are visible. Note however the strong low maturity anomaly (high OMAT value) evident in the walls of the crater. A similar feature is not observed in the CF image. Applying the OMAT correction given above nicely removes the ray pattern, but imposes a high CF value on the walls of the crater (Fig. 9c). This ring is solely the result of the very high OMAT value of the crater wall compared to the lack of this distinct anomaly in the CF image. This suggests a distinct difference in weathering effects between the two parameters, and the need for some mitigation in using OMAT for this correction.

The high albedo of the walls of Giordano Bruno would imply a relatively extreme thermal gradient within the surface, but the thermal conditions within the crater may alter the expectations applied to flat slopes. The very steep walls of this crater are viewing much less solid angle of cold space than a flat lying surface, and this may suppress the thermal gradient dependence on albedo relative to a flat surface. Regardless of the explanation, OMAT

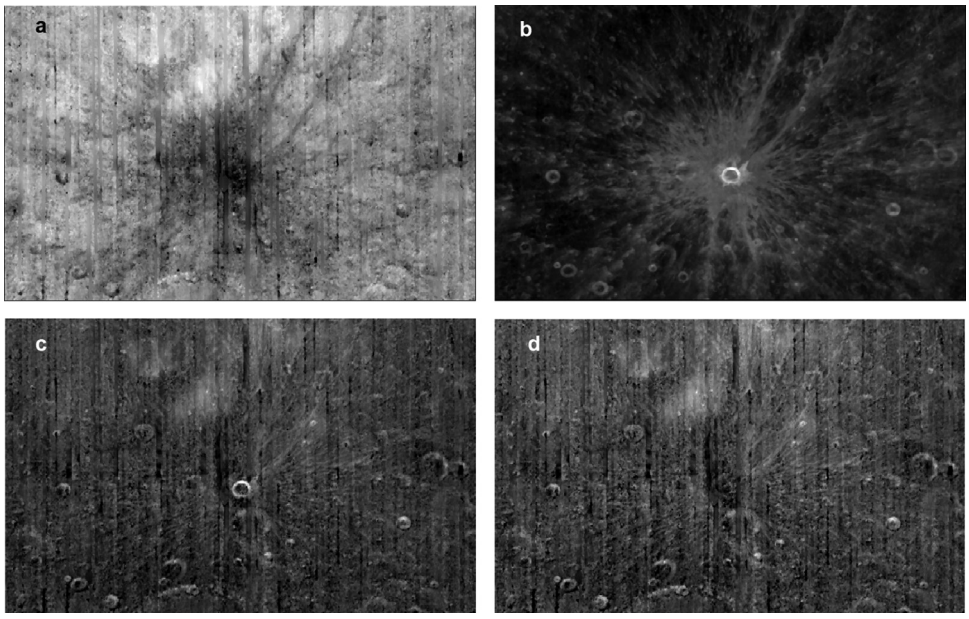

Fig. 9. Top left (a): CF image of Giordano Bruno showing a strong anomaly in its interior and ray pattern. Top right (b): OMAT image of Giordano Bruno crater showing the prominent ray pattern and a distinctive ring pattern from mass wasting on its steep walls. Bottom left (c): CF image corrected for space weathering. The ray pattern of Giordano Bruno has been largely eliminated, but a CF anomaly has been introduced at the walls of the crater. Bottom right (d): CF image adjusted for space weathering including lower limit to OMAT of 0.3. The anomalous ring has been eliminated.

overestimates the effect of space weathering at these locations. Our simple solution is to limit the OMAT value to 0.3 everywhere prior to correction, on the assumption that this overestimate at Giordano Bruno is consistent Moon wide. A consequence of this limitation is that the CF position of the least weathered surfaces are little adjusted by the application of OMAT, while the more space weathered surfaces are shifted toward values consistent with mineral mixtures. The result of the application of this refinement is shown in Fig. 9d. Note that the only visible difference between Fig. 9c and d are the steep walls of Giordano Bruno and two smaller nearby craters. The final correction is then:

$$CF_{Adjusted} = CF + (OMAT > 0.3) - 0.285 \quad (2)$$

We now examine a case in the lunar maria. The lunar swirl Reiner Gamma is an interesting case for understanding space weathering (Hood et al., 1979; Hood and Schubert, 1980; Blewett et al., 2011; Garrick-Bethell et al., 2011; Kramer et al., 2011; Denevi et al., 2014; Glotch et al., 2015; Hemingway et al., 2015) and the vicinity also features the nearby crater Reiner with steep walls brightened by mass wasting and exposure of fresh material. Fig. 10 shows CF (a), OMAT (b) and corrected CF (c,d) images of the Reiner Gamma Swirl as well as the crater Reiner. The swirl and Reiner as distinct low maturity anomalies, as are a number of small craters in the vicinity of Reiner. Reiner gamma shows as a subtle negative CF anomaly consistent with a less mature surface. The interior of Reiner is indistinct with an inconsistent pattern, while the small fresh craters nearby show local CF lows. Application of Eq. 2 results in Fig. 10c. The adjustment appears to have overcorrected the space weathering effect and both Reiner crater and Reiner Gamma show positive adjusted CF anomalies. We find that scaling OMAT by 0.5 produces an improved correction at Reiner Gamma and some of the small craters (Fig. 10d). This can indicate some change in the nature of space weathering in the maria relative to highlands, or alternatively an uncompensated bias in OMAT in representing maturity in the mare regions. For the present we are recommending the correction given in Eq. 2 pending further investigations.

Finally, we apply the space weathering correction (Eq. 2) to the global data set and present the results for the Copernican and Eratosthenian craters in Fig. 11. After the correction most of the Copernican and Eratosthenian crater deposits show CF positions consistent with the lunar highlands (in contrast to Fig. 3). Both populations have a long tail toward longer positions; these are consistent with their locations within the lunar maria.

5. Conclusions

Our findings indicate that space weathering affects the position of the Christiansen Feature position as measured by Diviner. Known lunar features associated with space weathering variations, in particular Copernican rayed craters and lunar swirls, have corresponding Christiansen Feature position anomalies. Prior spectral measurements of lunar soils with widely different degrees of space weathering measured under terrestrial ambient (isothermal) conditions indicated the spectral effects of space weathering would be small. However, under simulated lunar conditions a pair of Apollo 16 soils – 67701 and 66031 – that differ principally in degree of space weathering are substantially different spectrally, with shifts of Christiansen Feature wavelength consistent with Diviner observations.

We also observe a strong inverse correlation of albedo and the CF position. This suggests that albedo may have a strong influence on the Christiansen Feature wavelength position perhaps by affecting the thermal gradient. However, close examination of areas with known extreme composition or Christiansen Feature wavelength position (silica- and olivine-rich locations) deviate strongly from the overall lunar Christiansen Feature wavelength-albedo trend, showing that composition is a strong control on the measured lunar surface Christiansen Feature wavelength position and albedo is not the sole control on this parameter.

Use of the Christiansen Feature wavelength position data as currently available must take space weathering effects into account, but much of the lunar surface is fully mature and studies of mature surfaces should produce consistent results. Uncertainty in CF position when confined to mature surfaces is about 0.02 μm.

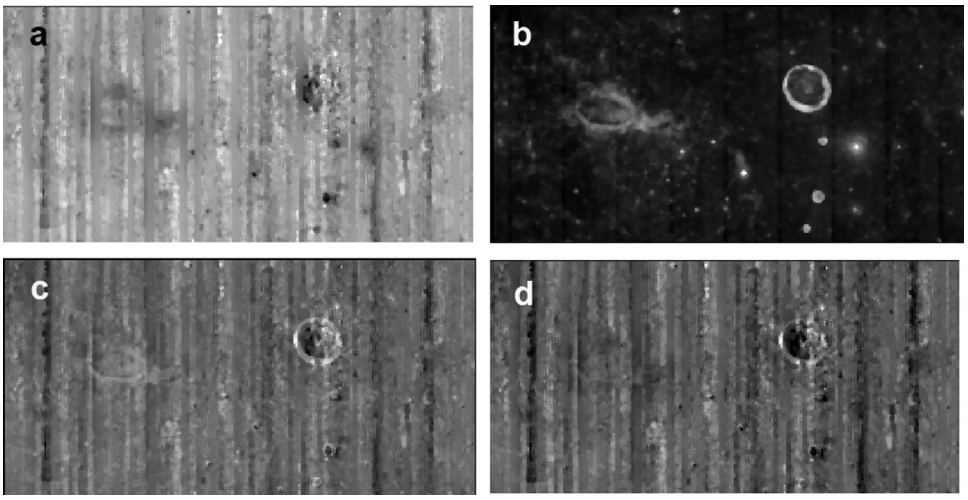

Fig. 10. Top left (a): CF image of the Reiner Gamma formation and Reiner crater. Reiner Gamma appears as a weak negative CF anomaly, and Reiner as a mottled feature. Negative CF anomalies are present at small fresh craters evident in the OMAT image. Top right (b): OMAT image of the same region as top left. Bottom left (c): CF image adjusted using OMAT and Eq. 2. The algorithm has overcorrected the maturity anomalies, leaving positive CF excursions at Reiner Gamma and at the walls of Reiner. Bottom right (d): CF adjusted with OMAT scaled by 0.5. Somewhat better correction is found at Reiner Gamma, but an anomaly at the walls of Reiner persists.

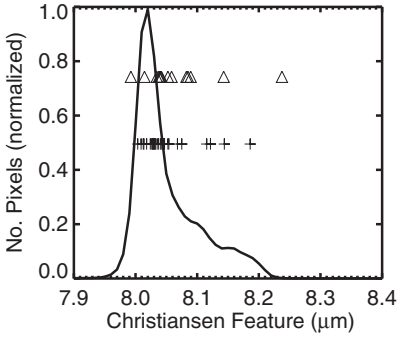

Fig. 11. Histogram of corrected CF values for the global data shown in Fig. 8. Triangles and plus signs are the CF values for all Copernican and Eratosthenian craters between 40 and 110 km in diameter respectively (y value is not significant). Both populations now straddle the main highland peak, and a long tail to toward long wavelengths represents craters in the maria. Compare with Fig. 3.

The near-IR derived OMAT parameter can be used to correct the CF data for the space weathering effect, but the results can be improved upon. Comparison of CF and OMAT suggest that in the least weathered areas the two parameters diverge in their response to space weathering. This could be an effect on thermal gradients of surfaces on steep slopes, or inherent problems with OMAT. The proposed correction is less effective in the lunar maria; future adjustments could improve it, such as imposing a composition-dependent scale factor.

The understanding of space weathering effects in the thermal infrared is just beginning and outlines of the issues are emerging. This paper has shown that thermal infrared spectroscopy is demonstrably affected by space weathering, but these effects can be mitigated to some extent. Empirical measurements in the laboratory have been an invaluable guide to understanding these effects, as has the limited theoretical work done.

Two major thermal infrared spectral experiments are planned for the near future (OTES on the OSIRIS-Rex mission to the dark asteroid Bennu and MERTIS on the BepiColumbo Mercury orbiter). Mercury exhibits very strong space weathering effects in the visible and near-IR, and in contrast to the Moon, shows very weak compositional variations in available spectral data, so the extraction of the compositional signal from MERTIS data will require special care. The spectral response of C-type materials to simulated space weathering is a topic of active research, but the lunar example is a caution that the asteroid may have properties contrary to expectations derived from laboratory experiments.

An effective, predictive model of the infrared spectral effects of space weathering on planetary materials will be an essential tool for drawing confident conclusions from these data. However, it is clear that a comprehensive understanding of space weathering on thermal infrared spectra of planetary materials is not yet in hand. The planned thermal spectral measurements of Mercury and Bennu suggest that ongoing efforts in this area have some urgency.

Acknowledgments

Work described in this paper was sponsored by the National Aeronautics and Space Administration's Lunar Reconnaissance Orbiter project under a contract to the University of California at Los Angeles, David A. Paige, Principal Investigator. This is Hawaii Institute of Geophysics and Planetology Publication Number 2192 and School of Ocean and Earth Sciences and Technology Publication Number 9630. The authors thank Douglas Hemingway and David Blewett for thoughtful reviews. The sponsor was not involved in the study design, in the collection, analysis or interpretation of data, in the writing of the report, or in the decision to submit the article for publication.

References

Allen, C.C., Greenhagen, B.T., Donaldson Hanna, K.L., et al., 2012. Analysis of lunar pyroclastic deposit FeO abundances by LRO Diviner. J. Geophys. Res. Planets 117, E00H28. doi:10.1029/2011JE003982.

Arnold, J.A., Glotch, T.D., Lucey, P.G., et al., 2016. Lunar olivine as seen by Diviner and M3: A comparison of MIR and VNIR spectral data. J. Geophys. Res. (submitted for publication).

Basilevsky, A.T., Head, J.W., 2012. Age of Giordano Bruno crater as deduced from the morphology of its secondaries at the Luna 24 landing site. Planet. Space Sci. 73 (1), 302–309.

Blewett, D.T., Coman, E.I., Hawke, B.R., et al., 2011. Lunar swirls: Examining crustal magnetic anomalies and space weathering trends. J. Geophys. Res. 116, E02002. doi:10.1029/2010JE003656.

Charette, M.P., McCord, T.B., Pieters, C.M., et al., 1974. Application of remote spectral reflectance measurements to lunar geology classification and determination of titanium content of lunar soils. J. Geophys. Res. 79, 1605–1613. doi:10.1029/JB079i011p01605.

Denevi, B.W., Robinson, M.S., Boyd, A.K., et al., 2014. Characterization of space weathering from Lunar reconnaissance orbiter camera ultraviolet observations of the Moon. J. Geophys. Res. Planets 119, 976–997. doi:10.1002/2013JE004527.

Dissly, R.W., Brown, R.H., Matson, D.L., 1990. Laboratory measurements of the solid-state greenhouse effect in glass beads. Proceedings of Abstracts of the Lunar and Planetary Science Conference, p. 295 Vol. 21, (abstract).

Donaldson Hanna, K.L., Greenhagen, B.T., Patterson, W.M. III, et al., Effects of varying environmental conditions on emissivity spectra of bulk lunar soils: Application to Diviner thermal infrared observations of the Moon. Icarus, (submitted for publication).

Donaldson Hanna, K.L., Thomas, I.R., Bowles, N.E., et al., 2012a. Laboratory emissivity measurements of the plagioclase solid solution series under varying environmental conditions. J. Geophys. Res. Planets 117 (E11). doi:10.1029/2012JE004184.

Donaldson Hanna, K.L., Wyatt, M.B., Thomas, I.R., et al., 2012b. Thermal infrared emissivity measurements under a simulated lunar environment: Application to the Diviner Lunar Radiometer Experiment. J. Geophys. Res. Planets 117 (E12).

Fischer, E.M., Pieters, C.M., 1994. Remote determination of exposure degree and iron concentration of lunar soils using VIS-NIR spectroscopic methods. Icarus 111 (2), 475–488.

Fischer, E.M., Pieters, C.M., 1995. Lunar surface aluminum and iron concentration from Galileo solid state imaging data, and the mixing of mare and highland materials. J. Geophys. Res. 100, 23279–23290. doi:10.1029/95JE02359.

Garrick-Bethell, I., Head, J.W., Pieters, C.M., 2011. Spectral properties, magnetic fields, and dust transport at lunar swirls. Icarus 212, 480–492. doi:10.1016/j.icarus.2010.11.036.

Glotch, T.D., Bandfield, J.L., Lucey, P.G., et al., 2015. Formation of lunar swirls by magnetic field standoff of the solar wind. Nat. Commun. 6, 6189. doi:10.1038/ncomms7189.

Glotch, T.D., Hagerty, J.J., Lucey, P.G., et al., 2011. The Mairan domes: Silicic volcanic constructs on the Moon. Geophys. Res. Lett. 38, L21204. doi:10.1029/2011GL049548.

Glotch, T.D., Lucey, P.G., Bandfield, J.L., et al., 2010. Highly silicic compositions on the Moon. Science 329, 1510–1513. doi:10.1126/science.1192148.

Gold, T., 1955. The lunar surface. Mon. Not. R. Astron. Soc. 115, 585–604. doi:10.1093/mnras/115.6.585.

Greenhagen, B.T., et al., 2011. The Diviner Lunar Radiometer compositional data products: Description and examples. In: Lunar and Planetary Science Conference, Vol. 42.

Greenhagen, B.T., Lucey, P.G., Wyatt, M.B., et al., 2010. Global silicate mineralogy of the Moon from the diviner lunar radiometer. Science 329, 1507–1509. doi:10.1126/science.1192196.

Hapke, B., 2001. Space weathering from Mercury to the asteroid belt. J. Geophys. Res. Planets 106, 10039–10073. doi:10.1029/2000JE001338.

Hawke, B.R., Blewett, D.T., Lucey, P.G., et al., 2004. The origin of lunar crater rays. Icarus 170, 1–16. doi:10.1016/j.icarus.2004.02.013.

Hemingway, D.J., Garrick-Bethell, I., Kreslavsky, M.A., 2015. Latitudinal variation in spectral properties of the lunar maria and implications for space weathering. Icarus 261, 66–79. doi:10.1016/j.icarus.2015.08.004.

Henderson, B.G., Jakosky, B.M., 1997. Near-surface thermal gradients and mid-IR emission spectra: A new model including scattering and application to real data. J. Geophys. Res. Planets 102, 6567–6580. doi:10.1029/96JE03781.

Hood, L.L., Coleman, P.J., Wilhelms, D.E., 1979. The Moon: Sources of the crustal magnetic anomalies. Science. 204, 53–57. doi:10.1126/science.204.4388.53.

Hood, L.L., Schubert, G., 1980. Lunar magnetic anomalies and surface optical properties. Science. 208, 49–51. doi:10.1126/science.208.4439.49.

Keller, L.P., McKay, D.S., 1997. The nature and origin of rims on lunar soil grains. Geochim. Cosmochim. Acta 61, 2331–2341. doi:10.1016/S0016-7037(97)00085-9.

Kramer, G.Y., Besse, S., Dhingra, D., et al., 2011. M 3 spectral analysis of lunar swirls and the link between optical maturation and surface hydroxyl formation at magnetic anomalies. J. Geophys. Res. 116, E00G18. doi:10.1029/2010JE003729.

Logan, L.M., Hunt, G.R., 1970. Emission spectra of particulate silicates under simulated lunar conditions. J. Geophys. Res. 75, 6539–6548. doi:10.1029/JB075i032p06539.

Logan, L.M., Hunt, G.R., Salisbury, J.W., et al., 1973. Compositional implications of Christiansen frequency maximums for infrared remote sensing applications. J. Geophys. Res. 78, 4983–5003. doi:10.1029/JB078i023p04983.

Lucey, P.G., Blewett, D.T., Taylor, G.J., et al., 2000. Imaging of lunar surface maturity. J. Geophys. Res. Planets 105, 20377–20386. doi:10.1029/1999JE001110.

Lucey, P.G., Paige, D.A., Greenhagen, B.T., et al., 2010. Diviner Christiansen feature position and visible albedo: Composition and space weathering implications. Proceedings of Lunar Planetary Science Conference XLI, #1600(abstract).

Morris, R.V., 1978. The surface exposure (maturity) of lunar soils: Some concepts and Is/FeO compilation. In: Proceedings of the 9th Lunar Planetary Science Conference, 2, pp. 2287–2297. (abstract).

Nash, D.B., Salisbury, J.W., 1991. Infrared reflectance spectra (2.2-15 μm) of plagioclase feldspars. Geophys. Res. Lett. 18, 1151–1154. doi:10.1029/91GL01008.

Nash, D.B., Salisbury, J.W., Conel, J.E., et al., 1993. Evaluation of infrared emission spectroscopy for mapping the Moon's surface composition from lunar orbit. J. Geophys. Res. 98, 23535–23552. doi:10.1029/93JE02604.

Noble, S.K., Pieters, C.M., Taylor, L.A., et al., 2001. The optical properties of the finest fraction of lunar soil: Implications for space weathering. Meteorit. Planet. Sci. 36, 31–42. doi:10.1111/j.1945-5100.2001.tb01808.x.

Nozette, S., Rustan, P., Pleasance, L.P., et al., 1994. The Clementine mission to the Moon: Scientific overview. Science 266, 1835–1839. doi:10.1126/science.266.5192.1835.

Ohtake, M., Haruyama, J., Matsunaga, T., et al., 2008. Performance and scientific objectives of the SELENE (KAGUYA) Multiband Imager. Earth, Planets Sp 60, 257–264. doi:10.1186/BF03352789.

Ohtake, M., Matsunaga, T., Haruyama, J., et al., 2009. The global distribution of pure anorthosite on the Moon. Nature 461, 236–240. doi:10.1038/nature08317.

Pieters, C.M., Taylor, L.A., Noble, S.K., et al., 2000. Space weathering on airless bodies: Resolving a mystery with lunar samples. Meteorit. Planet. Sci. 35, 1101–1107. doi:10.1111/j.1945-5100.2000.tb01496.x.

Salisbury, J.W., Basu, A., Fischer, E.M., 1997. Thermal infrared spectra of lunar soils. Icarus 130, 125–139. doi:10.1006/icar.1997.5809.

Taylor, L.A., Pieters, C.M., Keller, L.P., et al., 2001. Lunar mare soils: Space weathering and the major effects of surface-correlated nanophase Fe. J. Geophys. Res. Planets 106, 27985–27999. doi:10.1029/2000JE001402.

Thomas, I.R., Greenhagen, B.T., Bowles, N.E., et al., 2012. A new experimental setup for making thermal emission measurements in a simulated lunar environment. Rev. Sci. Instrum. 83, 124502. doi:10.1063/1.4769084.

Yamamoto, S., Nakamura, R., Matsunaga, T., et al., 2010. Possible mantle origin of olivine around lunar impact basins detected by SELENE. Nat. Geosci. 3, 533–536. doi:10.1038/ngeo897.